Journal of Drug Delivery Science and Technology 87 (2023) 104718

Contents lists available at ScienceDirect

Journal of Drug Delivery Science and Technology

journal homepage: www.elsevier.com/locate/jddst

Enhanced activity of a pluronic F127 formulated Pin1 inhibitor for ovarian cancer therapy

Gloria Saorin [a,b], Matteo Mauceri [a], Enrico Cavarzerani [a,b], Isabella Caligiuri [c], Giulia Bononi [d], Carlotta Granchi [d], Michele Bartoletti [e], Tiziana Perin [c], Tiziano Tuccinardi [d,f], Vincenzo Canzonieri [c,g], Muhammad Adeel [a], Flavio Rizzolio [a,c,*]

[a] Department of Molecular Sciences and Nanosystems, Ca'Foscari University of Venice, Venezia-Mestre, Italy
[b] Dotoctoral School in Science and Technology of Bio and Nanomaterials, Ca' Foscari University of Venice, Venezia-Mestre, Italy
[c] Pathology Unit, Centro di Riferimento Oncologico di Aviano (CRO) IRCCS, Aviano, Italy
[d] Department of Pharmacy, University of Pisa, Pisa, Italy
[e] Unit of Medical Oncology and Cancer Prevention, Department of Medical Oncology, Centro di Riferimento Oncologico di Aviano (CRO), IRCCS, Aviano, Italy
[f] Sbarro Institute for Cancer Research and Molecular Medicine, Center for Biotechnology, College of Science and Technology, Temple University, Philadelphia, PA, United States
[g] Department of Medical, Surgical and Health Sciences, University of Trieste, Trieste, Italy

1. Introduction

Worldwide cancer is the second cause of death exceeded only by cardiovascular diseases [1]. Ovarian cancer is the fifth cause of death in women and the principal of gynaecological cancer [2]. The number of ovarian cancers diagnosed in 2018 worldwide was estimated nearly of 300.000 with a number of deaths of about 185.000 [3]. The poor prognosis of ovarian cancer patients is due to a late diagnosis of the tumor. Around 63% of ovarian cancer cases are diagnosed at stage IV, which corresponds to a five-year survival rate of 27.6%, while tumor diagnosed at stage I has a survival rate of 92.4%. Indeed, the disease remains quite asymptomatic until it metastasizes [4]. The term ovarian cancer includes more than 30 different types of cancer, among which 85–90% are epithelial ovarian cancers [5]. The most common subtype of epithelial ovarian cancers is the serous carcinoma. The serous subtype is in the 90% of cases of high-grade tumors. For high-grade serous epithelial ovarian cancer (HGSOC), the standard line of treatments are surgery and platinum-based chemotherapy, however recurrence commonly occurs and in most cases the treatment of the relapse fails. In order to improve prevention, detection and treatment, a molecular characterization of ovarian cancer needs to be ameliorated. In this perspective, the role of Peptidyl-prolyl *cis*-trans isomerase NIMA-interacting 1 (Pin1) in HGSOC has been studied, demonstrating that its inactivation restrains tumor growth [6]. Pin1 is an enzyme made up by 163 amino acids, which has as target sequence a phosphorylated Ser/Thr-Pro motif and it is responsible for its enzymatic conversion between cis and trans conformation. Pin1 contains two important domains, the WW (two tryptophans conserved) and the PPIase domains. Both domains are involved in proline conversion but only the PPIase exerts catalytic activity [7]. The conformational changes due to Pin1 activity play a role in different cellular processes. In fact, the sequential events of the cell cycle process are regulated by the phosphorylation and dephosphorylation of various cell cycle-regulatory proteins and their post-phosphorylation modifications. Pin1 proved to negatively regulate cell cycle progression of normal cells delaying cell mitosis and arresting G2 phase by binding to different cell cycle-regulatory proteins including Wee1, cyclin D1, Cdc25C, Cyclin E, Myt1 and p27 [8]. Our group and others demonstrated that the inhibition of Pin1 is a promising strategy for cancer treatment since it is up regulated in cancer cells and cancer stem cells [8–11,38]. Furthermore, since cancer stem cells are a major cause of drug resistance, the inhibition of Pin1 is a powerful strategy to mitigate resistance arising from traditional chemotherapies [6]. Indeed, in 1998 Juglone was proved to work as Pin1 inhibitor and since then, different molecules have been studied both as covalent or non-covalent Pin1 inhibitors mainly targeting the PPIase domain, but few inhibitors bonding the WW domain were also developed [7]. Unfortunately, most of Pin1 inhibitors reported in literature showing anticancer activity, display unfavorable characteristics. For example, Juglone, arsenic trioxide, KPT-6566 and sulfopin are not suitable for in vivo application for Pin1 inhibition because of their lack in specificity and/or cell permeability [12–15]. Researchers are still trying to develop new potent Pin1 inhibitors by adopting drug discovery approaches focusing over the achievement of selective and preferably non covalent inhibitors [16–19]. Among the different classes of Pin1 inhibitors, compound C17

* Corresponding author. Department of Molecular Sciences and Nanosystems, Ca'Foscari University of Venice, Venezia-Mestre, Italy.
E-mail address: flavio.rizzolio@unive.it (F. Rizzolio).

https://doi.org/10.1016/j.jddst.2023.104718
Received 23 December 2022; Received in revised form 27 June 2023; Accepted 28 June 2023
Available online 16 July 2023

developed by Guo et al. was chosen for this work [19]. Indeed, C17 is a potent non-covalent inhibitor of Pin1 with a nanomolar enzymatic activity, invalidated by its low solubility and, more importantly, by a very low activity on cancer cells, probably due to an unfavorable interaction with cellular membrane receptors [18,19]. Beside these limiting factors arising from cells interaction, C17 is one of the most potent non covalent inhibitor developed, given that further modifications of the molecular structure, to ameliorate the in vivo activity, decrease the inhibitory power over the enzyme. In order to improve the pharmacological parameters of drugs, drug delivery systems can be exploited. Different types of nanoparticles constituted by a matrix encapsulating drugs can be used to improve important parameters such as solubility, cell permeability and stability. In cancer therapy, carriers can be inorganic such as metals or silica, or organic such as polymers or lipids. However, it is preferable to choose biocompatible carrier materials to avoid their toxicity related effect. In this work, a biocompatible polymer Pluronic F127® has been used to develop a nano formulation of C17. Pluronic F127® was chosen since it is approved by FDA, and being biocompatible it has been utilized to develop drug delivery systems applied from phytopharmaceuticals [20,21] to cancer therapies [22–24]. Polymeric formulation of C17 anticancer activity has been tested on different ovarian cancer cell lines and patient derived tumor organoids (PDTOs), which represent a more relevant human model [25–28,39,40].

2. Materials and methods

2.1. Polymeric formulation

Powder of Pluronic® F-127 (Cat no P2443) (F127) suitable for cell culture was purchased from Merck, Darmstadt, Germany. Chloroform (Cat no67-66-3) was purchased from Thermo Fisher Scientific, Waltham, MA, US. Water was purified with Milli-Q® (Millipak® 0.22 μm) system. Compound 17 (C17) was synthetized in our laboratory as previously reported [19].

2.2. Polymeric formulation protocol

The polymeric formulation protocol has been adapted from a previously reported thin film rehydration method [29], tested to obtain the higher content of C17. C17 (6 mg) was solubilized with F127 (24 mg) in chloroform (3 ml) to obtain a clear solution. Then the chloroform was removed by a rotary evaporation to obtain a thin film composed by the mixture of surfactant and C17. Thereafter the layer was hydrated by adding 6 ml of milli-Q water and sonicating for 15 min in bath sonicator and 10 min with probe sonicator (40% frequency, 2 mm tip). During both the sonication steps the sample was kept in an ice bath to avoid thermal damaging of the mixture. The obtained C17 polymeric water formulation is then referred as C17-F127-FP; when only F127 was used for the polymeric formulation protocol the sample was referred to as F127-FP.

2.3. C17 solubility measurement and quantification

The solubility of C17 was predicted by the "Chemicalize" software (Chemicalize.com; ChemAxon Ltd., Budapest, Hungary) and experimentally determined by mixing 1 mg/mL of drug powder in milli-Q water for 1 h. The solution was then centrifuged at 10000 rpm for 10 min to eliminate the insolubilized fraction and quantified. C17 was spectroscopically quantified using an Agilent 8453 spectrophotometer and a calibration plot, measuring its absorption at 286 nm (full scans of C17 solubilized in methanol at different concentrations are reported in Fig. 1S). The presence of F127 is not affecting the UV-VIS spectra of C17 (Fig. 2S) and therefore the absorption at 286 nm was used to quantify C17 concentration of both the samples prepared for the solubility measurement and the C17-F127-FP. The encapsulation efficiency% (EE %) was calculated as the ratio of the encapsulated C17 over the total amount of inhibitor used in the protocol, multiplied by 100. Percentage of drug loading capacity (DL%) was calculated, with the following formula, as lowest value by considering a total recovering of F127 from thin film, i.e. achieving a final concentration of 4 mg/ml.

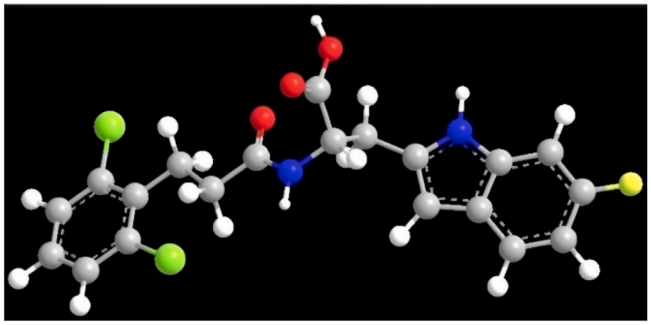

Fig. 1. C17 molecular structure.

$$DL\% = \frac{weight\ of\ encapsulated\ C17}{weight\ of\ encapsulated\ C17 + weight\ of\ F127} * 100$$

2.4. TEM analysis

About 25 μL of sample was dropped on a 400-mesh holey film grid and stained with 1% uranyl acetate (2 min). Then the sample was observed with a FEI Tecnai G2 transmission electron microscope operating at 100 kV (Hillsboro, Oregon, US). The images were taken with a Veleta digital camera (Olympus Soft Imaging System). Measurement of particles size was carried out by ImageJ (1.52a) software.

2.5. Dynamic light scattering analysis and zeta potential

Dynamic light scattering (DLS) and zeta potential analyses were performed by Zetasizer Nano particle analyzer (Malvern Panalytical, Malvern, UK).

2.6. XRD

Samples have been measured with X-ray diffractometer Empyrean (Malvern Panalytical, Worcestershire, UK). CuKα radiation was used, the diffractograms were recorded by setting a scan step size equal to 0.03939°, and scan range from 4 to 101°. The unit of measurement of the detected intensity is the number of pulses/second. Drug powder of C17 was directly measure using powder specimen holder, while C17-F127-FP and F127-FP concentrated solutions were deposited by repetitive step of dripping ad drying into Si low background sample holder until a visible film was obtained on the surface of the holder.

2.7. Drug release test

2 mL of C17-F127-FP was placed into a dialysis membrane Slide-A-Lyzer MINI Dialysis Device 20 k MWCO (Thermo Scientific, MA, USA) and dialyzed against DPBS kept at 37 °C and mixed. Aliquots of the solution were sampled at different time points and then C17 quantified through UV-VIS spectrometry. The results are expressed as release % calculated as follows.

$$Release\% = 100 * \frac{[C17]t0 - [C17]tx}{[C17]t0}$$

With [C17]t0 equal to starting drug concentration in C17-F127-FP sample used for the test, and [C17]tx equal to measured drug concentration in aliquots sampled at different time points.

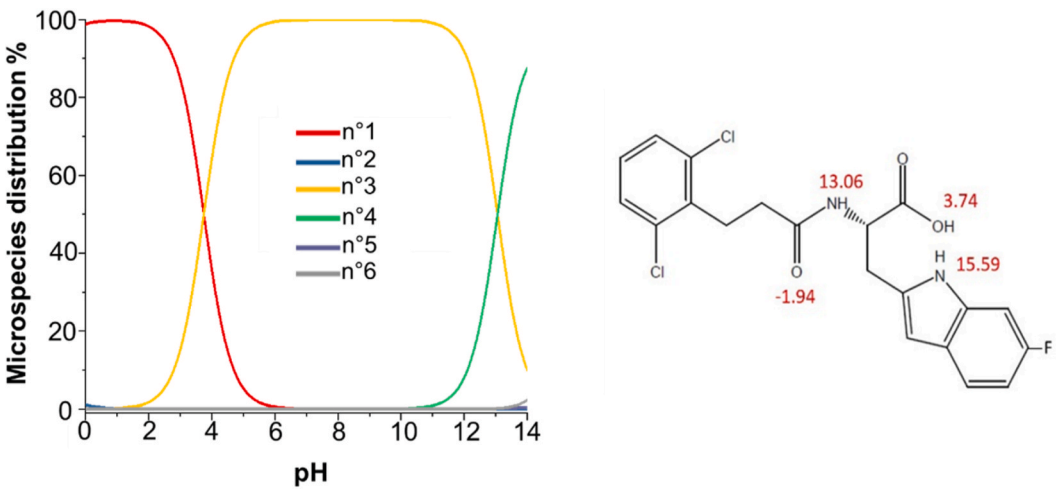

Fig. 2. (left) microspecies distribution as a function of pH; (right) C17 structure showing pKa values (in red). Predicted by Chemicalize software. (For interpretation of the references to colour in this figure legend, the reader is referred to the Web version of this article.)

2.8. Cell viability

Different ovarian cancer cell lines (A2780, A2780cis, OVCAR3, SKOV3 and KURAMOCHI) were grown in accordance with the supplier at 37 °C and 5% of CO2. 1 × 10^3 cells/well were seeded in 96-wells plates and treated with six different concentrations of C17 and C17-F127-FP (0.001, 0.01, 0.1, 1, 10, 100 μM) in triplicate. After 96 h, cell viability was measured using CellTiter-Glo (Promega, Madison, WI, USA) with BioTek Synergy H1. Logistical dose-response curves were used to calculate IC50 using GraphPad Prism (La Jolla, CA, US).

PDTO were obtained from totally anonymized specimens. However, biobank informed consent for research purposes was available to collect the samples at National Cancer Institute (CRO) of Aviano. HGSOC PDOs were cultured at 37 °C and 5% of CO2 followed a published protocol [27]. Cluster of PDOs were mixed in an appropriate volume of Matrigel and 2uL of this mixture were seeded in 96-wells plates and treated with six different concentrations of C17 and C17-F127-FP (0.32, 1.6, 8, 40, 200, 1000 μM) in four replicates. After 96 h, cell viability was measured using CellTiter-Glo 3D (Promega, Madison, WI, USA) with BioTek Synergy H1. Logistical dose-response curves were used to calculate IC50 using GraphPad Prism (La Jolla, CA, US).

2.9. Caspase 3/7 assay

1 × 10^3 OVCAR3 cells were seeded in 96-wells plates and treated with 25 and 50 μM of C17 and C17–F127– FP and 10 μM of cisplatin was used as a positive control. After 6 and 24 h of treatment, media was removed and Caspase-Glo® 3/7 (Promega, Madison, WI, USA) was added to each well. The luminescence was recorded after 30 min of incubation using BioTek Synergy H1.Cell viability and caspase 3/7 were performed in triplicate and the p-value was calculated using a two-tailed Student's t-test using GraphPad Prism (La Jolla, CA, US). p-values are expressed as follows: *P ≤ 0.05, **P ≤ 0.01, ***P ≤ 0.001 and ****P ≤ 0.0001.

3. Results and discussion

3.1. Compound properties

2-[3-(2,6-dichlorophenyl)propanamido]-3-(6-fluoro-1H-indol-2-yl) propanoic acid, referred as C17, is showed in Fig. 1. The molecule has a molecular weight of 423.27 g/mol. C17 belongs to a series of alkyl amide indole derivatives, which were developed with the aim of improving cellular permeability by decreasing the polarity of a group of benzimidazole-based Pin1 inhibitors. Indeed, C17 and the related compounds of this chemical class proved to have an increased solubility and cell permeability with respect to benzimidazole-based inhibitors, but lacked in cells activity probably due to the exclusion from cancer cells through PGP receptor efflux [19].

C17 properties have been predicted with the online platform Chemicalize and compared with experimentally determined and data previously reported in literature [19] (Table 1).

As can be seen in Table 1, the properties reported in literature, experimentally measured and predicted by the online platform are consistent. The solubility of the compound depends on pH and therefore, the values reported are affected by the considered condition. Basing on the intrinsic solubility, C17 is practically insoluble but the neutral form (microspecie n°1 in Fig. 2) subsides in favour of the mono anionic form generated by the dissociation of the carboxilic group (microspecie n°3 in Fig. 2) with a pH increment. Indeed, the solubility increases together with pH reaching 423 mg/ml over pH 10 (Fig. 3) when also the second acid proton start to dissociate from the amido group (pKa 13.06) generating the microspecie n°4 in Fig. 2. Other ionic microspecies generated from the dissociation of the indole acid proton (microspecie n°6 in Fig. 2) and the protonation of the carbonyl group (microspecie n°2 in Fig. 2) but are less prevalent. Accordingly, the hydrophilicity of the molecule increases with pH values (Fig. 3).

3.2. Formulation solubility and characterization

From the direct application of the polymeric formulation protocol, the final drug concentration is 0.71 ± 0.07 mg/ml (data obtained from a quadruplicate) in milli-Q water (which is equivalent to 71 ± 7 EE% and DL% of 15). Furthermore, the C17-F127-FP has been concentrated to achieve a stable solution with drug concentration equal to 5 mg/ml. Therefore, through the protocol the solubility of the drug is nearly three times the measured value in MQ water, and it can be concentrated since

Table 1
C17 chemical properties.

	Chemicalize	[19]	measured
solubility	Intrinsic 0.242 μg/ml (pH 6.5) 140 μg/ml	>100 μg/ml	240 ± 10 μg/ml
logP	4.32	3.5(experimentally determined)	n.d.
pKa (strongest)	3.74	3.9(experimentally determined)	n.d.
Isoelectric point	0.9	n.d.	n.d.

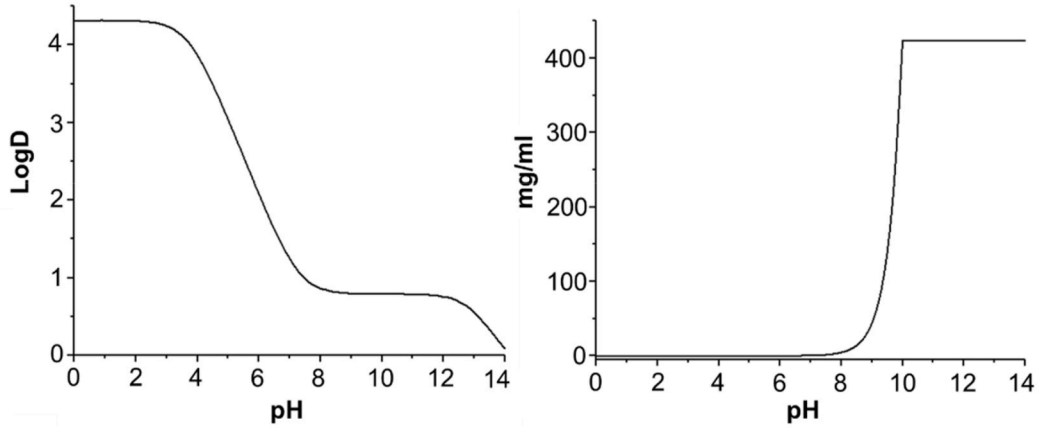

Fig. 3. (left) trend of logD; (right) trend of solubility as a function of pH, predicted by Chemicalize software.

twenty times more (at physiological pH).

In order to indagate the content of C17- F127-FP sample, it was analyzed with Zetasizer Nano particle analyzer. As can be seen in in Fig. 4, the C17-F127-FP contains two different populations of particles and indeed the global poly dispersion index is quite high reaching 0.54 (Table 1S). Zeta potential is negative (-10 ± 6 mV) due to the dissociation of the strongest acidic group in C17.

For clarifying the nature of the particles contained in the C17-F127-FP, TEM images of an aliquot of this sample were taken and are reported in Fig. 5. TEM images confirmed DLS results, indeed also in TEM images two different populations of particles can be seen: smaller regular spherical particles, as expected in the case of polymeric micelles, with a diameter of 23.9 ± 0.5 nm and bigger porous particles with an average diameter equal of 179 ± 13 nm.

The TEM analysis, in agreement with XRD data (Fig. 6), suggests that C17-F127-FP is in the amorphous state indeed scanning the grid only one crystal was seen (visible in the center of Fig. 5 A). The average diameters of the particles determined from TEM images (Table 2S) are compatible with DLS sizes determined by the two peaks, considering that DLS is measuring the hydrodynamic radius. Furthermore, the difference between DLS and TEM sizes is smaller for the polymeric micelles than for the bigger particles. This can arise from an enhanced deformation of these latest during the TEM grid preparation and therefore it might suggest that their porosity is due to a collapse, while their actual structure in solution is probably more homogeneous. In order to assess the role of the surfactant F127 on the nanoparticle formation, TEM images of a C17 water dispersion (C17-WD) and of a solution of F127 processed following the polymeric formulation protocol called F127-FP, were taken and reported in Fig. 5 B and C, respectively (data summarized in Table 2S). Both of samples are made of two different particles: C17-WD contains few micrometric crystals (average length of 1000 ± 300 nm) and spherical particles (16±1 nm) resembling micellar structures. F127-FP images show two populations of polymeric micelles; bigger spherical particles that tends to aggregate with an average diameter of 91 ± 4 nm and smaller ones, micelles, present in the background with an average diameter of 11.9 ± 0.7 nm. The porous particles present in C17-F127-FP must contained both C17 and F127 since no similar structures are present in F127-FP and neither in C17-WD both as morphology and size (Fig. 3S). Micelle sizes are affected by the mixing of the polymer and the drug. Indeed, in C17-F127-FP micelles are bigger if compared to micelles measured in the singular component of the mixture (Fig. 4S). This suggests the presence of the drug into the micelles in the C17-F127-FP sample.

XRD spectra of C17-F127-FP (red), C17 power (blue) and F127-FP (green) are shown in Fig. 6. The spectra of C17-F127-FP is clearly the combination of the other two, showing the broad peak present in C17 powder merged with sharp peaks due to F127. Since the only sharp peaks in C17-F127-FP are attributed to F127 the drug it is present mainly in amorphous phase, as for C17 drug powder which spectra shows only the broad peak. Thus, for C17 powder, the presence of crystals in TEM images might be due to recrystallization over the grid and are not prevalently in the sample since the drug clearly tends to be into an amorphous state.

C17-F127-FP stability over time was tested by measuring with DLS a

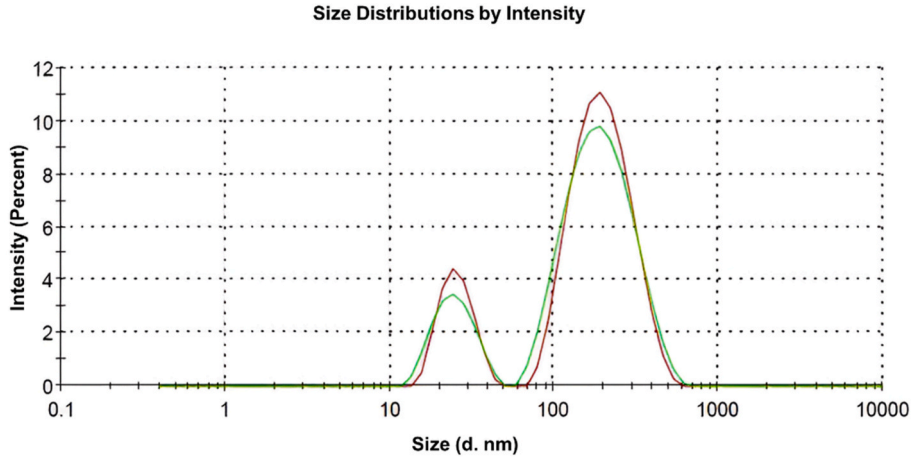

Fig. 4. Size distribution by intensity determined by DLS analysis of C17-F127-FP. Data are reported in Table 1S.

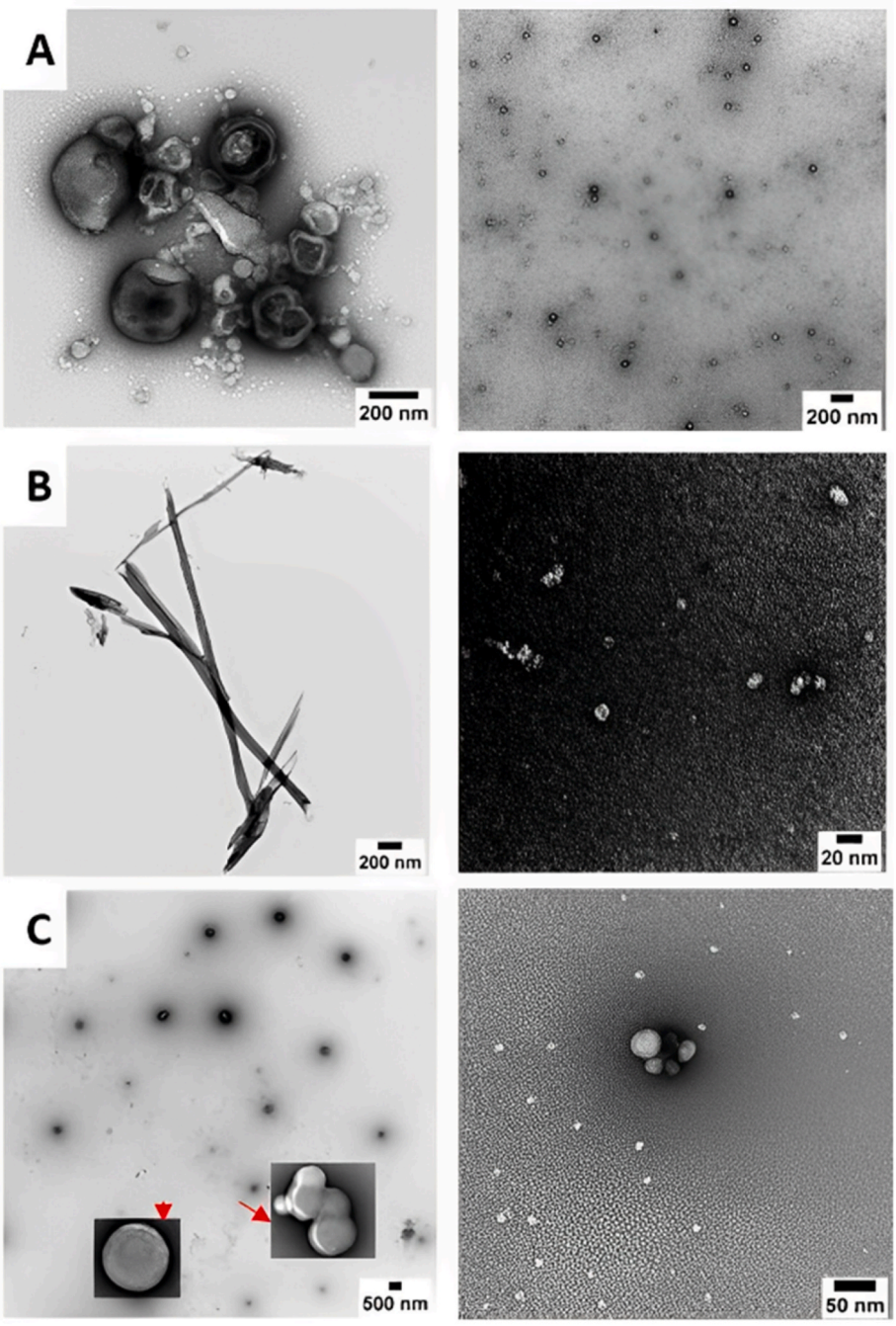

Fig. 5. TEM images of (A) C17-F127-FP, (B) C17-WD and (C) F127-FP. On right images, the micelles present in each sample are reported. Data are reported in Table2S.

tree months aged sample which present same particles curves with only a slight decrement of the average sizes (Fig. 5S). This prove that both particles are produced by stable interaction between their components, while the size decrement could be attribute to their partial dissolution, but gelation or aggregation can be excluded.

Pluronic® F127 is widely used for clinical applications as pharmaceutical adjuvant and nano carrier, approved by FDA, since it is biocompatible, promote long circulation period and is commercially available. Pluronic® F127 is a block copolymer composed by hydrophilic ethylene oxide (EO) and hydrophobic propylene oxide (PO) blocks with an A-B-A structure where A is EO. With this structure, many different Pluronic® polymers were created with different hydrophilicity achieved by the ratio between chain length of EO and PO. F127 is an hydrophile Pluronic® with high content in EO (EO100-PO65-EO100). Micelles are formed in water by self-assembly driven by hydrophobic interactions, indeed the polymer exposes the EO blocks while the center of the micelle is constituted by the hydrophobic PO block, where hydrophobic drugs could be entrapped. F127 is actually expected to generate spherical micelles with a hydrodynamic diameter ranging from 20 to 80 nm [30] with critical micelle concentration ranging from 0.1 to 3.17 mM [31]. Therefore, considering the F127 amount (0.32 mM) used in the polymeric formulation protocol micelle are expected. Micelles and polymeric nanoparticles are formed both in C17-F127-FP and F127-FP with differences between the two samples; indeed, when formulated alone F127, interestingly, showed both the presence of nanoparticles and micelles with size slightly smaller than what reported in literature

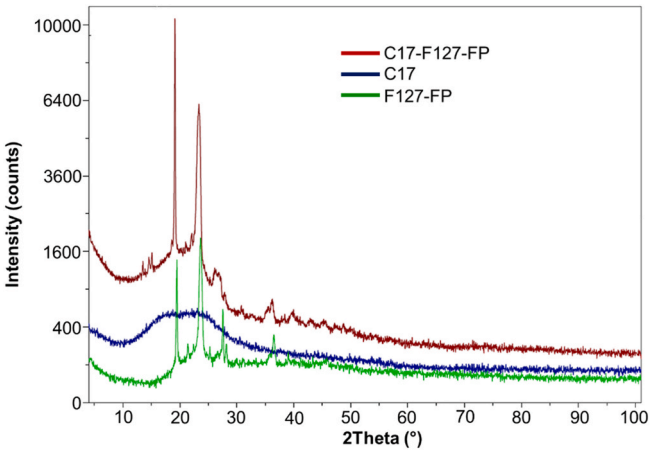

Fig. 6. XRD of C17 powder (blue), C17-F127-FP (red) and F127-FP (green). (For interpretation of the references to colour in this figure legend, the reader is referred to the Web version of this article.)

Table 2
cytotoxicity of C17 and C17-F127-FP on different ovarian cancer cell lines.

	IC_{50} (μM)				
Cell lines	A2780	A2780cis	OVCAR3	SKOV3	KURAMOCHI
F127	>100	>100	>100	>100	>100
C17	>100	>100	>100	>100	>100
C17-F127-FP	42.6 ± 2.6	45.0 ± 3.1	32.1 ± 5.2	31.3 ± 1.2	37.3 ± 4.5

[30]. Therefore, the formulation protocol and the presence of C17 are influencing the micellization and the formation of the polymeric particles, which are stable in the obtained solution. The polymeric formulation protocol, indeed, allows the production of a stable C17 nanoformulation suitable for drug delivery purposes by increasing its solubility.

3.3. C17 release from C17-F127-FP

In order to indagate the C17 release from the formulation an in vitro test, mimicking in vivo conditions, was developed, and the result is reported in Fig. 7. C17 undergo an initial burst release reaching 60% in 8h, while the remaining drug is then released within two days. This release trend can be explained by the initial release of C17 from micelles that are known to dissolve quickly [32] followed by the release from porous particle.

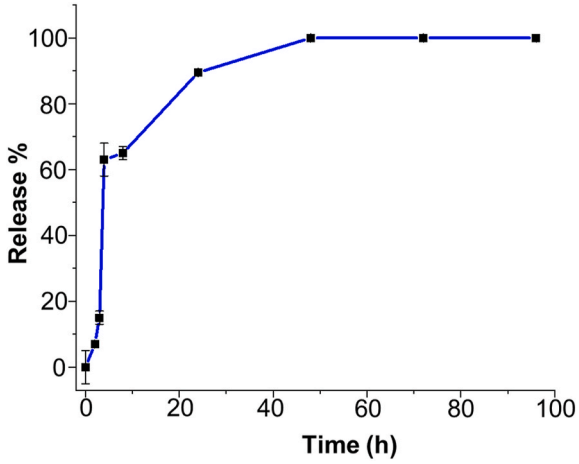

Fig. 7. graph of percentage of released C17 from C17-F127-FP over time.

3.4. Anticancer activity tests

Data reported in Table 2 confirmed what was defined in the original work about C17 inhibitory activity [19]: the drug lacks in cell activity.

Although C17 compound has no activity on all the cell lines tested, C17-F127-FP is active in the range of 31–45 μM. To strengthen the results, three HGSOC PDTOs were tested with the new polymeric formulation (Fig. 8). PDTO 1 is derived from ascites resistant to carboplatin. PDTO 2 and 3 derived from chemonaive primary surgery cancer tissues and are sensitive to platinum treatment. H&E evaluation and CA125 (cancer antigen 125), WT1 (Wilms' Tumor 1) and PAX8 (Paired box gene 8) biomarkers analyses confirmed that the characteristics of HGSOC are maintained (Fig. 6S).

PDTO 2 and 3 are sensitive to carboplatin, instead PDTO 1 is resistant as confirmed from the clinical data. C17 is inactive in all PDTOs. Differently, C17-F127-FP is effective on PDTO1 and barely active on PDTO 2 and 3 (Fig. 8A and B). Interestingly, as reported in Fig. 8C and D, high level of Pin1 expression is correlated with lower IC50 values suggesting that Pin1 inhibitors could be effective for the treatment of a subpopulation of HGSOC. Interestingly, Pin1 is more active on PDTO1 that is resistant to carboplatin.

Finally, the ability of C17-F127-FP to induce apoptosis was evaluated (Fig. 9). After 6 h of treatment, both formulations did not induce the activity of caspase 3 and 7. Differently, at 24 h only C17-F127-FP is effective and significantly activates the apoptotic pathway.

C17 was reported to have a good cell permeability (tested on Caco-2) and therefore the lack in cell activity was attributed to its exclusion from cells due to PGP receptor activity [19]. Pluronic ® polymers are known for being potent sensitizer of multiple drug resistance cells through polymer-cell interaction. Indeed, Pluronic® polymers were reported as inhibitors of ABC transporters, in particular PGP, MPR and BCRP and suppress the activity of ATPase transporters [33]. This activity over transporters is due to the alteration of the cell membrane lipid microenvironment by the polymers, since their amphiphilic structure can adhere and penetrate cell membranes. Hydrophilic Pluronic® polymers, such as F127, were reported to be able only to adhere to cell membrane but not insert and therefore not affecting the lipid packaging not being able to inhibit the transporters [30,33]. However, by adhering over cell membrane, F127 promotes drug permeation basing on the induced decrement in microviscosity, pore formation and flip-flop acceleration of membrane components [34]. On the other hand, other authors reported the increased action of anticancer drugs when formulated with F127 claiming that it is due to the inactivation of transporters [22,23] and moreover reporting the polymer action over cells promoting the interruption of essential process such as respiration [24]. Basing on the data reported in Table 2, F127 itself is not affecting cell viability but effectively enhancing C17 activity. Therefore, beside the fact that F127 interaction with cell membranes is still unclear, considering that the drug was proven to be able to permeate cell membrane but lacking in activity because of PGP efflux, it is possible to speculate that the enhanced anticancer activity of C17-F127-FP demonstrated by a decrement of IC50 values and enhanced apoptosis, is a further proof that also F127, as the more hydrophobic Pluronic® polymers, is affecting the transporter activity.

4. Conclusions

The polymeric formulation of the Pin1 inhibitor C17-F127-FP allows to obtain two populations of particles: micelles and porous particles that, by comparison with the components of the mixture, are probably both containing the drug. The presence of two different nanoparticles influences the release of the drug in the tumor site. Indeed, in literature is reported that nanomicelles having smaller size penetrate more rapidly into cells showing higher cellular uptake efficiency than bigger particles

A

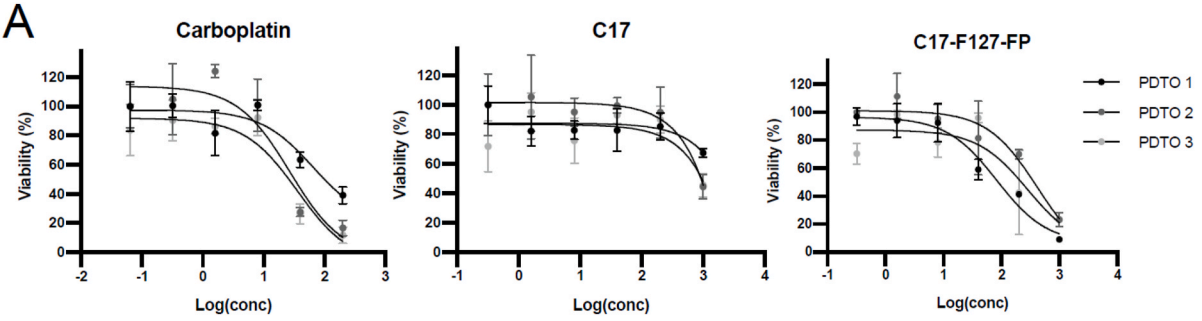

B

	PDTO 1 (IC_{50} µM)	PDTO 2 (IC_{50} µM)	PDTO 3 (IC_{50} µM)
Carboplatin	> 200	36,4 ± 11,4	39,9 ± 9,1
C17	> 1000	> 1000	> 1000
C17-F127-FP	76,9 ± 8,2	> 200	> 200

C

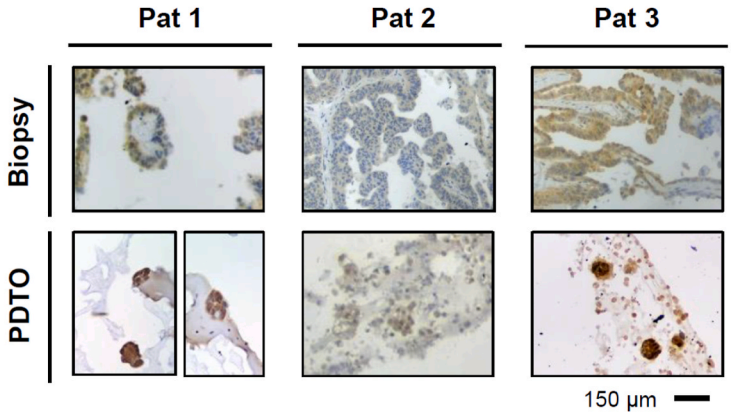

D

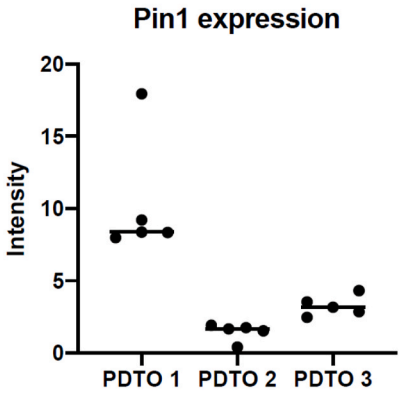

Fig. 8. (A) Dose-response curves of HGSOC Ascites patient (Pat 1) and two HGSOC PDTOs (Pat 2 and Pat 3) treated with Carboplatin, C17 and C17-F12-FP. (B) IC50 values (µM) of carboplatin, C17 and C17- F12-FP as reported in (A). Data were obtained from four replicates. The numbers represent mean and standard deviation. (C) Immunohistochemistry of Pin1 expression in parental and PDTO samples. (D) Distribution of intensity of Pin1 expression in HGSOC-PDTOs of Pat 1, Pat 2 and Pat 3. The line inside the values represents the median value. The results indicated that Pin1 is highly expressed in HGSOC-PDTOs of Pat 1 compared to Pat 2 and Pat 3 (<0.0126). p-value is calculated with «RM one-way ANOVA». H&E staining and Immunohistochemistry are reported in Fig. 3S.

[32] and guarantee a fast initial release [35]. That was proven by the release test of C17-F127-FP that showed an initial release, probably due to micelle dissolution, followed by the prolonged release from porous particles. Both particles when delivered into blood circulation, basing on their sizes [36], could eventually accumulate into tumoral sites by an enhanced permeation and retention effect. However, F127 micelles, were proved to release their content within first day (both in literature an in this work) and therefore before reaching the tumoral site [32]. Although, the possible release of the drug from micelles before reaching the tumor site might be useful to target and eliminate circulating cancer cells [37]. The stable dispersion derived from the polymeric formulation protocol, increased the solubility of C17 up to twenty times at physiological pH, but, more importantly, allows to demonstrate C17 activity over ovarian cancer cell lines and PDTOs proving the role of Pin1 in this type of gynaecological cancer and the role of F127 as promoting anti-cancer activity of drug almost certainly by exerting an inhibition over PGP who affected C17 action. This simple drug delivery system allowed to exert the activity of a non-covalent Pin1 inhibitor, which otherwise would be excluded from further application beside being among the most active over the enzyme. Further developments and improvements of the drug delivery system will be pursued but this work proved that C17 works over cells when nano formulated.

Financial disclosure

This research was funded by Fondazione AIRC (IG23566).

CRediT authorship contribution statement

Gloria Saorin: Conceptualization, Experimental data and Writing. **Matteo Mauceri:** Experimental data and Writing. **Enrico Cavarzerani:** Experimental data and Writing. **Isabella Caligiuri:** Formal analysis, Writing – review & editing. **Giulia Bononi:** Experimental data and Writing. **Carlotta Granchi:** Experimental data and Writing. **Michele Bartoletti:** Clinical data analysis, Writing. **Tiziana Perin:** Biological Samples, Review & Editing. **Tiziano Tuccinardi:** Experimental data and Writing. **Vincenzo Canzonieri:** Biological Samples, Review & Editing. **Muhammad Adeel:** Experimental data and Writing. **Flavio Rizzolio:** Conceptualization, Formal analysis, Writing – review & editing, Funding acquisition.

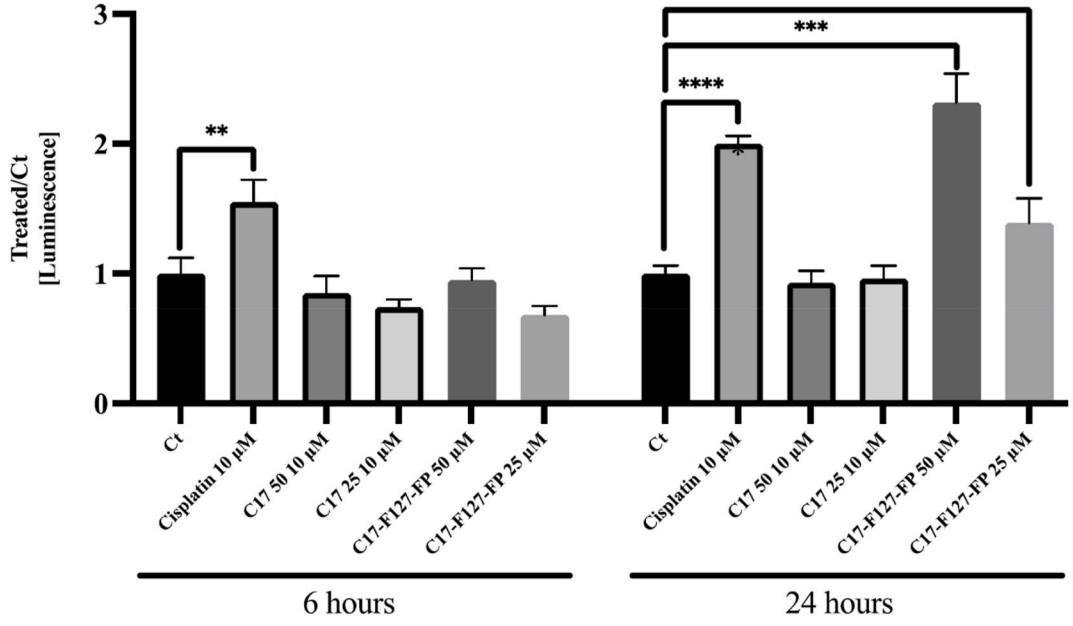

Fig. 9. caspase-3/7 activity in OVCAR3 cell line.

Declaration of competing interest

The authors declare that they have no known competing financial interests or personal relationships that could have appeared to influence the work reported in this paper.

Data availability

Data will be made available on request.

Appendix A. Supplementary data

Supplementary data to this article can be found online at https://doi.org/10.1016/j.jddst.2023.104718.

References

[1] H. Ritchie, M. Roser, Causes of Death, Published Online at OurWorldInData.Org, 2018.
[2] V.L. Seltzer, Ovarian cancer, in: Cancer Screening, CRC Press, 2021, pp. 431–440, https://doi.org/10.1201/9780429179587-19.
[3] Z. Khazaei, S.M. Namayandeh, R. Beiranvand, H. Naemi, S.M. Bechashk, E. Goodarzi, Worldwide incidence and mortality of ovarian cancer and Human Development Index (HDI): GLOBOCAN sources and methods 2018, J. Prevent. Med. Hygiene 62 (1) (2021) E174–E184, https://doi.org/10.15167/2421-4248/jpmh2021.62.1.1606.
[4] A. Saorin, E. di Gregorio, G. Miolo, A. Steffan, G. Corona, Emerging role of metabolomics in ovarian cancer diagnosis, in: Metabolites (Vol. 10, Issue 10, Pp. 1–15), MDPI AG, 2020, https://doi.org/10.3390/metabo10100419.
[5] S. Boussios, G. Zarkavelis, E. Seraj, I. Zerdes, K. Tatsi, G. Pentheroudakis, Non-epithelial ovarian cancer: elucidating uncommon gynaecological malignancies, in: Anticancer Research (Vol. 36, Issue 10, Pp. 5031–5042), International Institute of Anticancer Research, 2016, https://doi.org/10.21873/anticanres.11072.
[6] C. Russo Spena, L. de Stefano, S. Palazzolo, B. Salis, C. Granchi, F. Minutolo, T. Tuccinardi, R. Fratamico, S. Crotti, S. D'Aronco, M. Agostini, G. Corona, I. Caligiuri, V. Canzonieri, F. Rizzolio, Liposomal delivery of a Pin1 inhibitor complexed with cyclodextrins as new therapy for high-grade serous ovarian cancer, J. Contr. Release 281 (2018) 1–10, https://doi.org/10.1016/j.jconrel.2018.04.055.
[7] Y.M. Lee, Y.-C. Liou, Gears-in-motion: the interplay of WW and PPIase domains in Pin1, Front. Oncol. 8 (2018), https://doi.org/10.3389/fonc.2018.00469.
[8] C.-W. Cheng, E. Tse, PIN1 in cell cycle control and cancer, Front. Pharmacol. 9 (2018) 1367, https://doi.org/10.3389/fphar.2018.01367.
[9] C. Lucchetti, I. Caligiuri, G. Toffoli, A. Giordano, F. Rizzolio, The prolyl isomerase Pin1 acts synergistically with CDK2 to regulate the basal activity of estrogen receptor α in breast cancer, PLoS One 8 (2) (2013), e55355, https://doi.org/10.1371/journal.pone.0055355.
[10] F. Rizzolio, C. Lucchetti, I. Caligiuri, I. Marchesi, M. Caputo, A.J. Klein-Szanto, L. Bagella, M. Castronovo, A. Giordano, Retinoblastoma tumor-suppressor protein phosphorylation and inactivation depend on direct interaction with Pin1, Cell Death Differ. 19 (7) (2012) 1152–1161, https://doi.org/10.1038/cdd.2011.202.
[11] F. Rizzolio, I. Caligiuri, C. Lucchetti, R. Fratamico, V. Tomei, G. Gallo, A. Agelan, G. Ferrari, G. Toffoli, A.J. Klein-Szanto, A. Giordano, Dissecting Pin1 and phospho-pRb regulation, J. Cell. Physiol. 228 (1) (2013) 73–77, https://doi.org/10.1002/jcp.24107.
[12] C. Dubiella, B.J. Pinch, K. Koikawa, D. Zaidman, E. Poon, T.D. Manz, B. Nabet, S. He, E. Resnick, A. Rogel, E.M. Langer, C.J. Daniel, H.-S. Seo, Y. Chen, G. Adelmant, S. Sharifzadeh, S.B. Ficarro, Y. Jamin, B. Martins da Costa, N. London, Sulfopin is a covalent inhibitor of Pin1 that blocks Myc-driven tumors in vivo, Nat. Chem. Biol. 17 (9) (2021) 954–963, https://doi.org/10.1038/s41589-021-00786-7.
[13] E. Campaner, A. Rustighi, A. Zannini, A. Cristiani, S. Piazza, Y. Ciani, O. Kalid, G. Golan, E. Baloglu, S. Shacham, B. Valsasina, U. Cucchi, A.C. Pippione, M.L. Lolli, B. Giabbai, P. Storici, P. Carloni, G. Rossetti, F. Benvenuti, G. del Sal, A covalent PIN1 inhibitor selectively targets cancer cells by a dual mechanism of action, Nat. Commun. 8 (1) (2017), 15772, https://doi.org/10.1038/ncomms15772.
[14] J.D. Moore, A. Potter, Pin1 inhibitors: pitfalls, progress and cellular pharmacology, Bioorg. Med. Chem. Lett 23 (15) (2013) 4283–4291, https://doi.org/10.1016/j.bmcl.2013.05.088.
[15] L. Hennig, C. Christner, M. Kipping, B. Schelbert, K.P. Rücknagel, S. Grabley, G. Küllertz, G. Fischer, Selective inactivation of parvulin-like peptidyl-prolyl *cis/trans* isomerases by Juglone, Biochemistry 37 (17) (1998) 5953–5960, https://doi.org/10.1021/bi973162p.
[16] G. Poli, M. di Stefano, J.A. Estevez, F. Minutolo, C. Granchi, A. Giordano, S. Parisi, M. Mauceri, V. Canzonieri, M. Macchia, I. Caligiuri, T. Tuccinardi, F. Rizzolio, New PIN1 inhibitors identified through a pharmacophore-driven, hierarchical consensus docking strategy, J. Enzym. Inhib. Med. Chem. 37 (1) (2022) 145–150, https://doi.org/10.1080/14756366.2021.1979970.
[17] B.J. Pinch, Z.M. Doctor, B. Nabet, C.M. Browne, H.-S. Seo, M.L. Mohardt, S. Kozono, X. Lian, T.D. Manz, Y. Chun, S. Kibe, D. Zaidman, D. Daitchman, Z. C. Yeoh, N.E. Vangos, E.A. Geffken, L. Tan, S.B. Ficarro, N. London, N.S. Gray, Identification of a potent and selective covalent Pin1 inhibitor, Nat. Chem. Biol. 16 (9) (2020) 979–987, https://doi.org/10.1038/s41589-020-0550-9.
[18] C. Russo Spena, L. De Stefano, G. Poli, C. Granchi, M. El Boustani, F. Ecca, G. Grassi, M. Grassi, V. Canzonieri, A. Giordano, T. Tuccinardi, I. Caligiuri, F. Rizzolio, Virtual screening identifies a PIN1 inhibitor with possible antiovarian cancer effects, J. Cell. Physiol. (2019), https://doi.org/10.1002/jcp.28224.
[19] C. Guo, X. Hou, L. Dong, J. Marakovits, S. Greasley, E. Dagostino, R. Ferre, M. Catherine Johnson, P.S. Humphries, H. Li, G.D. Paderes, J. Piraino, E. Kraynov, B.W. Murray, Structure-based design of novel human Pin1 inhibitors (III): optimizing affinity beyond the phosphate recognition pocket, Bioorg. Med. Chem. Lett 24 (17) (2014) 4187–4191, https://doi.org/10.1016/j.bmcl.2014.07.044.
[20] N.-D.H. Luu, L.H. Dang, H.M. Bui, T.T.T. Nguyen, B.T. Nguyen, L.S. Hoang, N. Q. Tran, Nanoencapsulation of chromolaena odorata extract using pluronic F127 as an effectively herbal delivery system for wound healing, 2021, J. Nanomater. (2021) 1–12, https://doi.org/10.1155/2021/6663986.
[21] D. van Thoai, D.T. Nguyen, L.H. Dang, N.H. Nguyen, V.T. Nguyen, P. Doan, B. T. Nguyen, le Van Thu, N.N. Tung, T.N. Quyen, Lipophilic effect of various pluronic-grafted gelatin copolymers on the quercetin delivery efficiency in these self-assembly nanogels, J. Polym. Res. 27 (12) (2020) 369, https://doi.org/10.1007/s10965-020-02216-z.

[22] J. Hou, J. Wang, E. Sun, L. Yang, H.M. Yan, X. bin Jia, Z.H. Zhang, Preparation and evaluation of icariside II-loaded binary mixed micelles using Solutol HS15 and Pluronic F127 as carriers, Drug Deliv. 23 (9) (2016) 3248–3256, https://doi.org/10.3109/10717544.2016.1167270.

[23] E.v. Batrakova, S. Li, A.M. Brynskikh, A.K. Sharma, Y. Li, M. Boska, N. Gong, R. L. Mosley, V.Y. Alakhov, H.E. Gendelman, A.v. Kabanov, Effects of pluronic and doxorubicin on drug uptake, cellular metabolism, apoptosis and tumor inhibition in animal models of MDR cancers, J. Contr. Release 143 (3) (2010) 290–301, https://doi.org/10.1016/j.jconrel.2010.01.004.

[24] D.D. Guo, H.S. Moon, R. Arote, J.H. Seo, J.S. Quan, Y.J. Choi, C.S. Cho, Enhanced anticancer effect of conjugated linoleic acid by conjugation with Pluronic F127 on MCF-7 breast cancer cells, Cancer Lett. 254 (2) (2007) 244–254, https://doi.org/10.1016/j.canlet.2007.03.007.

[25] N. v Tzouras, T. Scattolin, A. Gobbo, S. Bhandary, F. Rizzolio, E. Cavarzerani, V. Canzonieri, K. van Hecke, G.C. Vougioukalakis, C.S.J. Cazin, S.P. Nolan, A green synthesis of carbene-metal-amides (CMAs) and carboline-derived CMAs with potent in vitro and ex vivo anticancer activity, ChemMedChem 17 (13) (2022), e202200135, https://doi.org/10.1002/cmdc.202200135.

[26] C. Granchi, G. Bononi, R. Ferrisi, E. Gori, G. Mantini, S. Glasmacher, G. Poli, S. Palazzolo, I. Caligiuri, F. Rizzolio, V. Canzonieri, T. Perin, J. Gertsch, A. Sodi, E. Giovannetti, M. Macchia, F. Minutolo, T. Tuccinardi, A. Chicca, Design, synthesis and biological evaluation of second-generation benzoylpiperidine derivatives as reversible monoacylglycerol lipase (MAGL) inhibitors, Eur. J. Med. Chem. 209 (2021), 112857, https://doi.org/10.1016/j.ejmech.2020.112857.

[27] O. Kopper, C.J. de Witte, K. Lõhmussaar, J.E. Valle-Inclan, N. Hami, L. Kester, A. V. Balgobind, J. Korving, N. Proost, H. Begthel, L.M. van Wijk, S.A. Revilla, R. Theeuwsen, M. van de Ven, M.J. van Roosmalen, B. Ponsioen, V.W.H. Ho, B. G. Neel, T. Bosse, H. Clevers, An organoid platform for ovarian cancer captures intra- and interpatient heterogeneity, Nat. Med. 25 (5) (2019) 838–849, https://doi.org/10.1038/s41591-019-0422-6.

[28] S.J. Hill, B. Decker, E.A. Roberts, N.S. Horowitz, M.G. Muto, M.J. Worley, C. M. Feltmate, M.R. Nucci, E.M. Swisher, H. Nguyen, C. Yang, R. Morizane, B. S. Kochupurakkal, K.T. Do, P.A. Konstantinopoulos, J.F. Liu, J. v Bonventre, U. A. Matulonis, G.I. Shapiro, A.D. D'Andrea, Prediction of DNA repair inhibitor response in short-term patient-derived ovarian cancer organoids, Cancer Discov. 8 (11) (2018) 1404–1421, https://doi.org/10.1158/2159-8290.CD-18-0474.

[29] J. Park, B. Sun, Y. Yeo, Albumin-coated nanocrystals for carrier-free delivery of paclitaxel, J. Contr. Release 263 (2017) 90–101, https://doi.org/10.1016/j.jconrel.2016.12.040.

[30] A. v Kabanov, E. v Batrakova, V.Y. Alakhov, P luronic block copolymers for overcoming drug resistance in cancer, in: Advanced Drug Delivery Reviews, vol. 54, 2002. www.elsevier.com/locate/drugdeliv.

[31] R.K. Thapa, F. Cazzador, K.G. Grønlien, H.H. Tønnesen, Effect of curcumin and cosolvents on the micellization of Pluronic F127 in aqueous solution, Colloids Surf. B Biointerfaces 195 (2020), https://doi.org/10.1016/j.colsurfb.2020.111250.

[32] Y. Liu, S. Fu, L. Lin, Y. Cao, X. Xie, H. Yu, M. Chen, H. Li, Redox-sensitive Pluronic F127-tocopherol micelles: synthesis, characterization, and cytotoxicity evaluation, Int. J. Nanomed. 12 (2017) 2635–2644, https://doi.org/10.2147/IJN.S122746.

[33] D.Y. Alakhova, A.v. Kabanov, Pluronics and MDR reversal: an update, in: Molecular Pharmaceutics (Vol. 11, Issue 8, American Chemical Society, 2014, pp. 2566–2578, https://doi.org/10.1021/mp500298q.

[34] H. Park, K. Na, Conjugation of the photosensitizer Chlorin e6 to pluronic F127 for enhanced cellular internalization for photodynamic therapy, Biomaterials 34 (28) (2013) 6992–7000, https://doi.org/10.1016/j.biomaterials.2013.05.070.

[35] C. Sirotti, I. Colombo, M. Grassi, Modelling of drug-release from poly-disperse microencapsulated spherical particles, J. Microencapsul. 19 (5) (2002) 603–614, https://doi.org/10.1080/02652040210141075.

[36] L. Niu, E. Jang, A. Lin Chin, R. Tong, External stimuli-responsive nanomedicine for cancer immunotherapy, in: Reference Module in Materials Science and Materials Engineering, Elsevier, 2021, https://doi.org/10.1016/B978-0-12-822425-0.00026-9.

[37] L. Valdivia, L. García-Hevia, M. Bañobre-López, J. Gallo, R. Valiente, M. López Fanarraga, Solid lipid particles for lung metastasis treatment, Pharmaceutics 13 (1) (2021) 93, https://doi.org/10.3390/pharmaceutics13010093.

[38] R. la Montagna, I. Caligiuri, P. Maranta, C. Lucchetti, L. Esposito, M.G. Paggi, G. Toffoli, F. Rizzolio, A. Giordano, Androgen receptor serine 81 mediates Pin1 interaction and activity, Cell Cycle 11 (18) (2012) 3415–3420, https://doi.org/10.4161/cc.21730.

[39] T. Scattolin, E. Bortolamiol, F. Visentin, S. Palazzolo, I. Caligiuri, T. Perin, V. Canzonieri, N. Demitri, F. Rizzolio, A. Togni, Palladium(II)-η3 -allyl complexes bearing N-trifluoromethyl N-heterocyclic carbenes: a new generation of anticancer agents that restrain the growth of high-grade serous ovarian cancer tumoroids, Chemistry (Weinheim an Der Bergstrasse, Germany) 26 (51) (2020) 11868–11876, https://doi.org/10.1002/chem.202002199.

[40] T. Scattolin, E. Bortolamiol, S. Palazzolo, I. Caligiuri, T. Perin, V. Canzonieri, N. Demitri, F. Rizzolio, L. Cavallo, B. Dereli, M. v Mane, S.P. Nolan, F. Visentin, The anticancer activity of an air-stable Pd(I)-NHC (NHC = N-heterocyclic carbene) dimer, Chem. Commun. 56 (81) (2020) 12238–12241, https://doi.org/10.1039/d0cc03883k.